The Discovery of Broad P Cygni X-ray Lines from Circinus X-1 with the *CHANDRA* High Energy Transmission Grating Spectrometer

W. N. Brandt[1] and N. S. Schulz[2]

Received ________________________; accepted ________________________

Accepted for publication in The Astrophysical Journal Letters

[1]Department of Astronomy and Astrophysics, 525 Davey Laboratory, The Pennsylvania State University, University Park, PA, 16802.

[2]Center for Space Research, Massachusetts Institute of Technology, Cambridge, MA 02139.

ABSTRACT

We present the first grating-resolution X-ray spectra of the X-ray binary Cir X-1, obtained with the High Energy Transmission Grating Spectrometer on *Chandra*. These reveal a rich set of lines from H-like and/or He-like Ne, Mg, Si, S and Fe detected with a high signal-to-noise ratio. The lines are broad (± 2000 km s^{-1}) and show P Cygni profiles. The absorption components of the lines extend to low velocity, and they have about the same widths and strengths as the corresponding emission components. The widths of the X-ray P Cygni lines are comparable to that of the broad component of the strong, asymmetric Hα line from Cir X-1, suggesting that the two phenomena may be related. We discuss outflow models and propose that the P Cygni profiles may arise in the moderate temperature ($\sim 5 \times 10^6$ K) region of the wind from an X-ray heated accretion disk. This basic picture strengthens the idea that the accretion disk in Cir X-1 is viewed in a relatively edge-on manner, and it suggests that Cir X-1 is the X-ray binary analog of a Broad Absorption Line quasar.

Subject headings: stars: individual (Cir X-1) — stars: neutron — X-rays: stars — binaries: close — accretion: accretion disks — techniques: spectroscopic

1. Introduction

The most sensitive indicators of mass loss from cosmic sources are the resonance absorption lines of abundant ions. In the ultraviolet, for example, these lines have been used to study outflows in objects ranging from stars to quasars. Prior to the launch of the *Chandra* X-ray Observatory (e.g., Weisskopf et al. 2000), however, X-ray spectrometers generally lacked the resolution and sensitivity needed to study resonance line absorption by the outflows from most cosmic objects. Resonance absorption line studies in the X-ray band offer a number of attractive features: (1) the continuum driving the ionization is often directly visible, (2) the atomic physics of the relevant ions is often relatively simple, and (3) unlike ultraviolet photons, X-rays are not easily destroyed in dusty environments.

The mysterious X-ray binary Cir X-1 is thought to contain a neutron star that can radiate at up to super-Eddington levels near the periastron passage ('zero phase') of its 16.5-day orbital cycle (e.g., Tennant, Fabian & Shafer 1986; Inoue 1989), and its accretion disk is probably viewed in a relatively edge-on manner (e.g., Brandt et al. 1996). The fact that it can radiate with high luminosity relative to its Eddington luminosity ($L/L_{\rm Edd}$) makes it a natural system in which to expect observable outflows, due to the larger amount of photon pressure available per unit gravitational mass. Indeed, the broad component (up to 2000 km s^{-1} FWHM) of the strong, asymmetric Hα line from Cir X-1 has been interpreted as arising in an outflow from regions near the neutron star (e.g., Whelan et al. 1977; Johnston, Fender & Wu 1999); the broad component of the Hα line is blueshifted relative to the narrow component. Furthermore, the system appears to emit radio jets and is embedded in a synchrotron nebula (e.g., Stewart et al. 1993; Fender et al. 1998). Finally, we note a convergence of opinion that the system is probably a low-mass X-ray binary based on photometry and variability of the optical counterpart (e.g., Stewart et al. 1991; Glass 1994), its orbital period and apparent space velocity (Brandt & Podsiadlowski 1996; Tauris et al. 1999), its correlated X-ray spectral and timing properties (e.g., Shirey, Bradt & Levine 1999), and the observed type 1 X-ray bursts (Tennant et al. 1986).

2. Observations and Data Analysis

Cir X-1 was observed using the High Energy Transmission Grating Spectrometer (HETGS; C.R. Canizares et al., in preparation) on *Chandra* starting at 22:09:50 UT on

2000 February 29 (see Figure 1).[3] The total integration time was 32 ks, and the observation was continuous. The observation start time corresponds to phase 0.99 using the ephemeris discussed by Glass (1994).

The HETGS carries two types of transmission gratings, the Medium Energy Grating (MEG) and the High Energy Grating (HEG). It allows high-resolution spectroscopy from ≈ 1.2–31 Å (≈ 0.4–10 keV) with a peak spectral resolution at ≈ 12 Å of $\lambda/\Delta\lambda \approx 1000$ for HEG 1st order. The resolution for higher orders improves by a factor of n for the nth order, but the spectral bandpass and efficiency are reduced for these orders. In this analysis we mostly utilize the MEG and HEG 1st order as well as the MEG 3rd order spectra.

The dispersed spectra were recorded with an array of 6 Charge Coupled Devices (CCDs) which are part of the Advanced CCD Imaging Spectrometer (ACIS; G.P. Garmire et al., in preparation).[3] To avoid CCD frame 'dropouts' due to telemetry saturation, we blocked the 0th order image with a 'spatial window' and shut off the two peripheral CCDs (S0 and S5). The omission of the peripheral CCDs could be tolerated because Cir X-1 is heavily absorbed by the interstellar column density ($N_{\rm H} \approx 2 \times 10^{22}$ cm^{-2}; e.g., Predehl & Schmitt 1995) and offers hardly any flux above ≈ 15 Å (e.g., Morrison & McCammon 1983). The brightness of Cir X-1 also required additional mitigation efforts for 'photon pile-up' effects. We applied a 'subarray' during the observation that reduced the CCD frame time to 1.7 s. The remaining pile-up effects caused the 1st order spectra below ≈ 10 Å (MEG) and ≈ 6 Å (HEG) to be depleted of photons, which then populate the higher order spectra at shorter wavelengths. Below 7 Å the MEG 1st order spectrum is so depleted that we will not use it further in this analysis. The MEG 3rd order spectrum is pile-up free from 2.3–9 Å (1.4–5.4 keV). Most of the lines we present below are not or are only moderately

[3]For additional information on the HETGS and ACIS see the *Chandra* Proposers' Observatory Guide at http://asc.harvard.edu/udocs/docs.

affected by pile-up.

Due to a misalignment of the applied subarray during the observation, only half of the dispersed spectra were fully recorded; we only have negative orders in the MEG and positive orders in the HEG complete. The *Chandra* X-ray Center (CXC) provided aspect-corrected level 1 event lists via its standard pipeline processing.

The determination of the 0th order image position is crucial for the calibration of the wavelength scales because it defines their zero point. We calculated this position by fitting the dispersed images of the MEG and HEG and by determining the intersections of these fits with the 0th order 'read-out trace' on the S3 CCD. The fits of the MEG and HEG were consistent to within 0.3 detector pixels, which translates into a zero point accuracy of 0.004 Å for the MEG -1st order and 0.002 Å for the HEG $+1$st order. The overall wavelength calibration is good to $\approx 0.1\%$ and mostly depends on uncertainties in the positions of the CCD chip gaps, which currently are ± 0.5 pixels. For most of the spectral features analyzed here there is only one gap involved leaving us with an overall worst case uncertainty in the scale of 0.008 Å for MEG -1st order, 0.005 Å for HEG $+1$st order, and 0.003 Å for MEG -3rd order.

We then processed the events into final event lists using CXC software, and we used custom software and FTOOLS to produce our final grating spectra. After standard grade selection, we have a total of 1.35×10^6 events in MEG -1st order, 1.52×10^6 events in HEG $+1$st order, and 3.84×10^5 events in MEG -3rd order. We corrected our final grating spectra for instrumental effects (e.g., energy dependent photon detection efficiency and gaps between the CCDs) using aspect-corrected exposure maps.

From the MEG -3rd order spectrum we determined a mean 2–8 keV flux of 1.8×10^{-8} erg cm^{-2} s^{-1}. This was calculated by fitting the *ASCA* continuum model of Brandt et al. (1996) to the 2.3–6.2 Å (2–5.4 keV) spectrum (where pile-up is unimportant) and then extrapolating the result to the 2–8 keV band. The observed flux is within the range that has recently been seen by *RXTE* (Shirey et al. 1999) at zero phase. Even for a fairly small distance of ≈ 6 kpc (see §3 of Stewart et al. 1993 and Case & Bhattacharya 1998), the 2–8 keV luminosity is $L_{2-8} \gtrsim 9.6 \times 10^{37}$ erg s^{-1} (corrected for interstellar absorption); hence for a $M = 1.4\ M_{\odot}$ neutron star with $L_{\rm Edd} = 1.3 \times 10^{38}(M/M_{\odot})$ erg s^{-1} we find $L_{2-8}/L_{\rm Edd} \gtrsim 0.5$ (note there is certainly substantial X-ray luminosity below 2 keV as well). Figure 2 shows the resulting HEG +1st and MEG −1st order spectra. These reveal a rich set of highly significant lines from H-like and/or He-like Ne, Mg, Si, S and Fe. The lines are broad (± 2000 km s^{-1}) and show P Cygni profiles (see Figure 3).

Table 1 gives a list of the lines identified with P Cygni profiles; many of these have two or more independent detections (see Figure 3 for an example). We used the line list presented in Mewe, Gronenschild & van den Oord (1985) to determine the line wavelengths and transition types. Most measured wavelengths agree to within 0.01 Å with the predicted wavelengths. Some wavelengths are measured to be slightly lower, which may be attributed to the fact that some of the profiles are broadened and not entirely symmetric. The 'peak-to-valley' distances for the P Cygni profiles are a measure of the broadening of the lines. Table 1 shows that the widths are quite significant (0.02–0.10 Å), well above the resolution of the HETGS. While there is evidence for line variability over time, P Cygni profiles are persistently present.

3. Discussion

The observed X-ray P Cygni profiles are most naturally interpreted as arising in a high-velocity outflow from the Cir X-1 system. Several properties of the profiles deserve note. First of all, the absorption troughs extend to low velocities; this suggests that we are seeing the region in which the outflow is accelerated, rather than, for example, just a shell of material that has already attained its terminal velocity. Secondly, the strengths of the emission and absorption components are comparable when integrated over the whole observation. Finally, the best-defined profiles look fairly smooth and continuous down to the resolution limit of the HETGS; at least down to this limit there is no evidence for strong shell-like density enhancements or other inhomogeneities in the outflow. The size of the Cir X-1 system is uncertain but is thought to be $\sim 5 \times 10^7$ km (e.g., Tauris et al. 1999), so the characteristic time for the outflow to cross the system is ~ 0.5 days.

As mentioned in §1, an outflow from the Cir X-1 system has already been invoked to explain the broad component of its Hα line (Johnston et al. 1999). The widths of the X-ray P Cygni profiles are quite consistent with the FWHM of the broad component of Hα, suggesting that these two phenomena may be related; ultraviolet P Cygni profiles and optical Hα emission are often seen together from stars with high mass loss rates (see §2.3 of Lamers & Cassinelli 1999). Johnston et al. (1999) argued that the broad Hα line component arises in a strong, anisotropic outflow driven by the radiation pressure from the neutron star. In their model, this outflow must be optically thick (to Hα photons) to explain the broad blue wing of the line (the redshifted emission being obscured by the outflow itself).

The observed P Cygni profiles are broadly consistent with such an outflow model, although this outflow must be fairly dense to avoid becoming completely ionized by the large X-ray luminosity of Cir X-1. In particular, the ionization parameter $\xi = L/nr^2$ must be $\lesssim 1000$ erg cm s^{-1} so that the ions listed in Table 1 can survive (see Kallman & McCray 1982).[4] If we take the launching radius (i.e., onset radius) of the outflow to be $r_{\rm launch} \approx 10^5$ km, so that its observed terminal velocity, $v_{\rm t}$, is comparable to the escape

[4]In the definition of ξ, L is the ionizing luminosity, n is the electron number density, and r is the distance to the ionizing radiation source.

velocity, $v_{\rm esc}$, at $r_{\rm launch}$, we require $n_{\rm launch} \gtrsim 10^{15}$ cm^{-3} (we consider the plausible case of outflows launched from larger radii where $v_{\rm t} > v_{\rm esc}$ below). For comparison, the expected density of the accretion disk at this radius is $\approx 2 \times 10^{18}$ cm^{-3}, so the outflow-to-disk density contrast seems plausible (compare with Figure 2 of Raymond 1993).[5] To allow the survival of H I (for Hα) in the outflow, $\xi \lesssim 1$ erg cm s^{-1} and hence $n_{\rm H\ I} \gtrsim 10^{18}$ cm^{-3} is required; such a high density outflow would be surprising, so it seems likely that most of the Hα emission is formed at a larger distance in the outflow or in the accretion disk (see Mignani, Caraveo & Bignami 1997).

Based on the X-ray spectral variability properties of Cir X-1, Brandt et al. (1996) argued that its accretion disk is flared and viewed in a relatively edge-on manner. X-rays emitted in the inner part of such a system can heat the surface of the disk farther out, producing a corona and thermally driven wind (e.g., Begelman, McKee & Shields 1983). The outflow revealed by our X-ray P Cygni profiles might well be this wind, although for this high $L/L_{\rm Edd}$ system radiation pressure acting on lines (in addition to Compton heating) is likely to be important. Raymond (1993) has examined atomic processes in the context of this scenario, and his calculations show that at distances of $\approx 10^5$–10^6 km there is a significant (subtending ~ 3–20°), moderate temperature ($\sim 5 \times 10^6$ K) region where atomic heating and cooling processes dominate over Compton processes. Significant line emission is expected from this region, and in fact most of the lines we list in Table 1 are those predicted to be strong by Raymond (1993). Thus, our favored interpretation for the observed X-ray P Cygni profiles is that they arise in the intermediate temperature region of the wind from an accretion disk viewed in a relatively edge-on manner. Cir X-1 then

---

[5]We have calculated the disk density following §5.6 of Frank, King & Raine (1992) with a neutron star mass of $M = 1.4\ M_\odot$, a mass accretion rate of $\dot{M} = 1.5 \times 10^{18}$ gm s^{-1}, and a viscosity parameter of $\alpha = 0.1$.

becomes an X-ray binary analog of a Broad Absorption Line quasar. At smaller radii, wind and coronal material are likely to be heated to the Compton temperature and thus completely ionized. An appealing physical possibility is that the electron scatterer discussed in §4.1 of Brandt et al. (1996) is just this material. Similar highly ionized gas has been invoked in some models for Broad Absorption Line quasars (e.g., the 'hitchhiking gas' of Murray et al. 1995).

Despite the general attractiveness of the above picture, we must note a potential difficulty: for a launching radius with $v_{\rm t} \approx v_{\rm esc}$, the quantity $N_{\rm H,launch} = \int_{r_{\rm launch}}^{\infty} n\,dr = n_{\rm launch} r_{\rm launch} \gtrsim 10^{25}$ cm^{-2} is so large that the implied column density through the wind is optically thick to electron scattering [here we assume that the wind has a radial extent $\gg r_{\rm launch}$ and that $n = n_{\rm launch}(r_{\rm launch}/r)^2$]. Most line photons attempting to traverse the wind would then be Compton scattered out of the line. Shielding of the wind from the full X-ray continuum may alleviate this problem by allowing a significant reduction in $n_{\rm launch}$ (see Begelman & McKee 1983). Alternatively, increasing $r_{\rm launch}$ helps because $N_{\rm H,launch} \propto r_{\rm launch}^{-1}$ when we require $\xi \lesssim 1000$ erg cm s^{-1} and thus $n_{\rm launch} \gtrsim L/(r_{\rm launch}^2\ 1000$ erg cm s^{-1}); in this case significant radiation pressure driving may be needed since $v_{\rm t} > v_{\rm esc}$. $r_{\rm launch}$ cannot be $\gg 10^6$ km as the disk probably has an outer radius $\lesssim 3 \times 10^6$ km (see Figure 3 of Tauris et al. 1999). Finally, clumping of the wind might also help because when clumping is present $\xi = Lf/nr^2$ where f is the volume filling factor. We note that Iaria et al. (2000) have recently found evidence for a large ionized column density ($\sim 10^{24}$ cm^{-2}) along the line of sight even when Cir X-1 is radiating at high luminosity; this material may be the same that makes the P Cygni lines. We are presently examining these issues in further detail.

While we cannot rigorously rule out the possibility that the X-ray P Cygni lines arise in a wind from the companion star, we consider this unlikely. First of all, the large wind velocity (± 2000 km s^{-1}) implied by the profiles would require a high-mass secondary for the system (for an overview see §2.7 of Lamers & Cassinelli 1999), provided the presence of the radiating compact object does not lead to a substantially faster wind from the companion than would otherwise be expected. However, as mentioned in §1, the bulk of the evidence suggests a low-mass X-ray binary nature. Furthermore, the large X-ray luminosity of Cir X-1 should completely ionize an O star wind out to $\gtrsim 5 \times 10^6$ km (compare with Boroson et al. 1999), while the observed P Cygni profiles suggest that we are seeing the acceleration region of the outflow.

To our knowledge, these are the first reported X-ray P Cygni profiles from an X-ray binary. Hopefully X-ray P Cygni profiles will be identified and studied in other systems to provide geometrical and physical insight into the flows of material near Galactic compact objects.

We thank all the members of the *Chandra* team for their enormous efforts, and we thank J. Chiang, A.C. Fabian, S.C. Gallagher, S. Kaspi, R.A. Wade, and an anonymous referee for helpful discussions. We gratefully acknowledge the financial support of CXC grant GO0-1041X (WNB, NSS), the Alfred P. Sloan Foundation (WNB), and Smithsonian Astrophysical Observatory contract SV1-61010 for the CXC (NSS).

REFERENCES

Begelman, M.C., McKee, C.F. & Shields, G.A. 1983, ApJ, 271, 70

Begelman, M.C. & McKee, C.F. 1983, ApJ, 271, 89

Boroson, B., Kallman, T., McCray, R., Vrtilek, S. & Raymond, J. 1999, ApJ, 519, 191

Brandt, W.N. & Podsiadlowski, Ph. 1995, MNRAS, 274, 461

Brandt, W.N., Fabian, A.C., Dotani, T., Nagase, F., Inoue, H., Kotani, T. & Segawa, Y. 1996, MNRAS, 283, 1071

Case, G.L. & Bhattacharya, D. 1998, ApJ, 504, 761

Fender, R., Spencer, R., Tzioumis, T., Wu, K., van der Klis, M., van Paradijs, J. & Johnston, H. 1998, ApJ, 506, L121

Frank, J., King, A. & Raine, D. 1992, Accretion Power in Astrophysics (Cambridge Univ. Press, Cambridge)

Glass, I. 1994, MNRAS, 268, 742

Iaria, R., Burderi, L., Di Salvo, T., La Barbera, A. & Robba, N. R. 2000, ApJ, in press (astro-ph/0009183)

Inoue, H. 1989, in Proc. 23rd ESLAB Symp. on Two Topics in X-ray Astronomy, ed. N.E. White, J. Hunt & B. Battrick (Paris: ESA Publications), 109

Johnston, H.M., Fender, R. & Wu, K. 1999, MNRAS, 308, 415

Kallman, T.R. & McCray, R. 1982, ApJS, 50, 263

Lamers, H.J.G.L.M. & Cassinelli, J.P. 1999, Introduction to Stellar Winds (Cambridge Univ. Press, Cambridge)

Mewe, R., Gronenschild, E.H.B.M. & van den Oord, G.H.J. 1985, A&AS, 62, 197

Mignani, R., Caraveo, P.A. & Bignami, G.F. 1997, A&A, 323, 797

Morrison, R. & McCammon, D. 1983, ApJ, 270, 119

Murray, N., Chiang, J., Grossman, S.A. & Voit, G.M. 1995, ApJ, 451, 498

Predehl, P. & Schmitt, J.H.M.M. 1995, A&A, 293, 889

Raymond, J.C. 1993, ApJ, 412, 267

Shirey, R.E., Bradt, H.V. & Levine, A.M. 1999, ApJ, 517, 472

Stewart, R.T., Nelson, G.J., Penninx, W., Kitamoto, S., Miyamoto, S. & Nicholson, G.D. 1991, MNRAS, 253, 212

Stewart, R.T., Caswell, J.L., Haynes, R.F. & Nelson, G.J., 1993, MNRAS, 261, 593

Tauris, T.M., Fender, R.P., van den Heuvel, E.P.J., Johnston, H.M. & Wu, K. 1999, MNRAS, 310, 1165

Tennant, A.F., Fabian, A.C. & Shafer, R.A. 1986, MNRAS, 221, 27P

Weisskopf, M.C., Tananbaum, H.D., Van Speybroeck, L.P. & O'Dell, S.L. 2000, Proc. SPIE, in press (astro-ph/0004127)

Whelan, J.A.J., et al. 1977, MNRAS, 181, 259

This manuscript was prepared with the AAS LaTeX macros v5.0.

TABLE 1

X-ray P Cygni lines from Cir X-1

Ion Name	Isoelectronic seq. and transition[a]	Predicted λ (Å)[b]	Measured λ (Å)[c]	$\Delta\lambda$ (Å)[d]
Fe XXVI	H-like (Lyα)	1.78	1.78	0.02
Fe XXV	He-like	1.85	1.85	0.02
S XVI	H-like (Lyα)	4.73	4.72	0.03
S XV	He-like	5.04	5.04	0.03
Si XIV	H-like (Lyβ)	5.22	5.21	0.03
Si XIV	H-like (Lyα)	6.18	6.17	0.03
Mg XII	H-like (Lyγ)	6.74	6.73	0.04
Mg XII	H-like (Lyα)	8.42	8.40	0.06
Ne X	H-like (Lyδ)	9.48	9.48	0.09
Fe XXIV	Li-like	10.63	10.63	0.10
Ne X	H-like (Lyα)	12.13	12.11	0.06

[a]We list the transition here if it can be written compactly; for the other transitions see Tables 1 and 3 of Mewe et al. (1985).

[b]From Mewe et al. (1985).

[c]Measured intersection of the P Cygni profile (between the emission maximum and absorption minimum) with a local continuum fit. The measurement accuracy corresponds to about 1 data bin (i.e., ± 0.0025 Å).

[d]Measured 'peak-to-valley' distances for the P Cygni profiles.

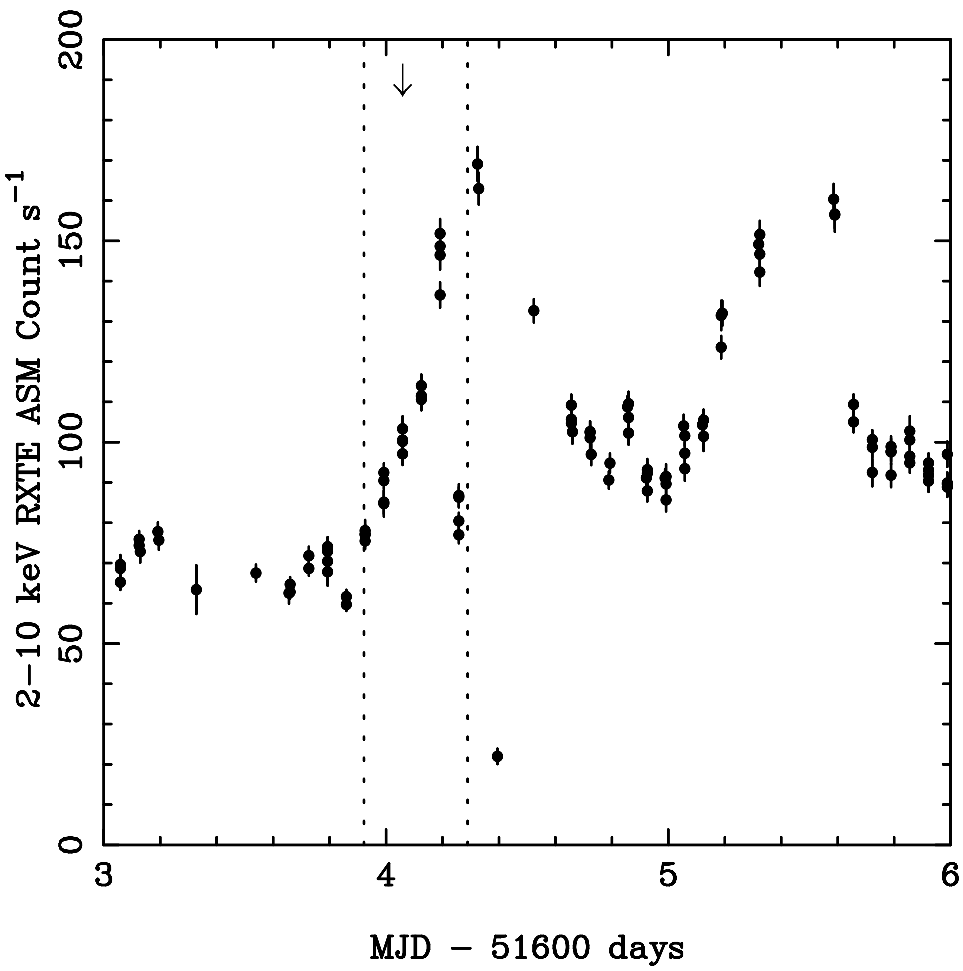

Fig. 1.— *RXTE* All-Sky Monitor (ASM) light curve of Cir X-1 around the time of our *Chandra* observation. The start and stop times of our *Chandra* observation are denoted by dotted vertical lines. The downward pointing arrow shows the zero-phase time of Cir X-1. For comparison, the count rate of the Crab in the *RXTE* ASM is ≈ 75 count s^{-1}.

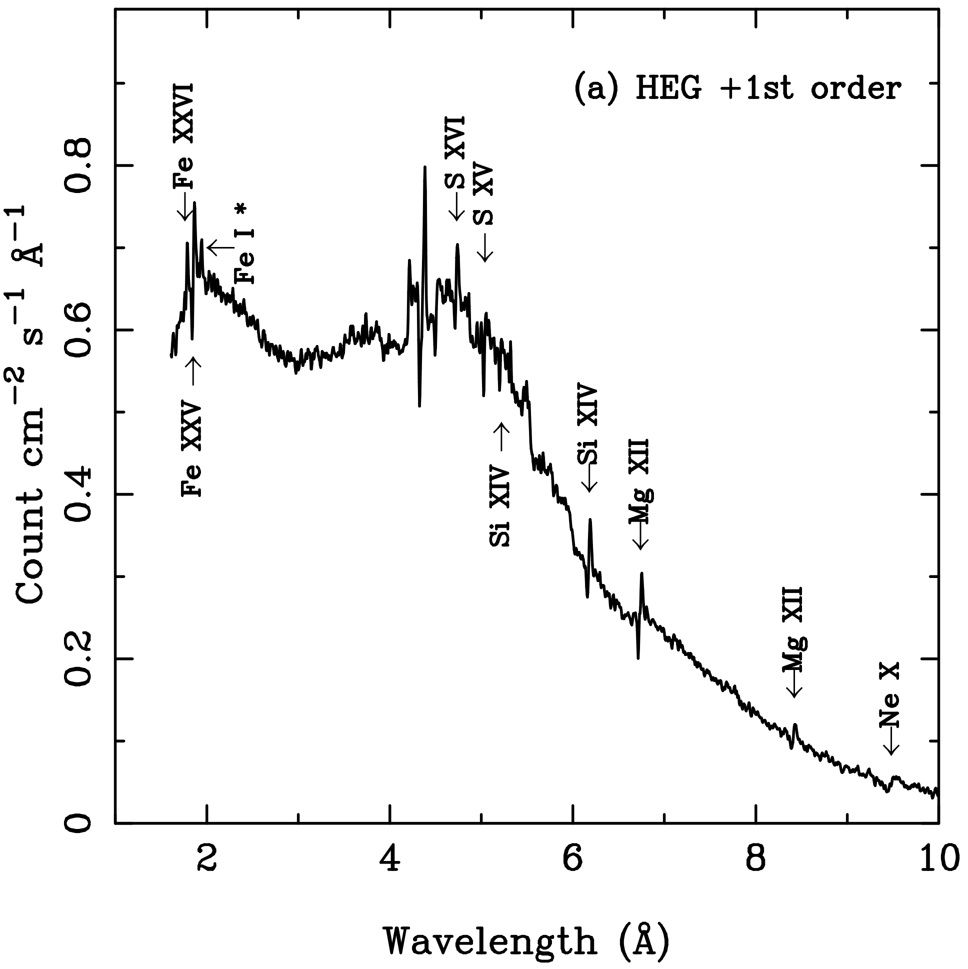

Fig. 2.— Exposure corrected (a) HEG +1st order and (b) MEG −1st order spectra of Cir X-1 with a spectral binning of 0.005 Å. These spectra have been smoothed with a 'boxcar' filter of width 3 bins, and they have not been corrected for the effects of interstellar absorption. We have marked all the P Cygni type spectral lines that are detected with $> 5\sigma$ significance and that are mostly free from contamination effects (we do not detect a P Cygni profile from Fe I so this line is starred). The feature at 4.31 Å corresponds to S XV, but it is not marked because its amplitude is strongly affected by uncertainties in the CCD gap correction.

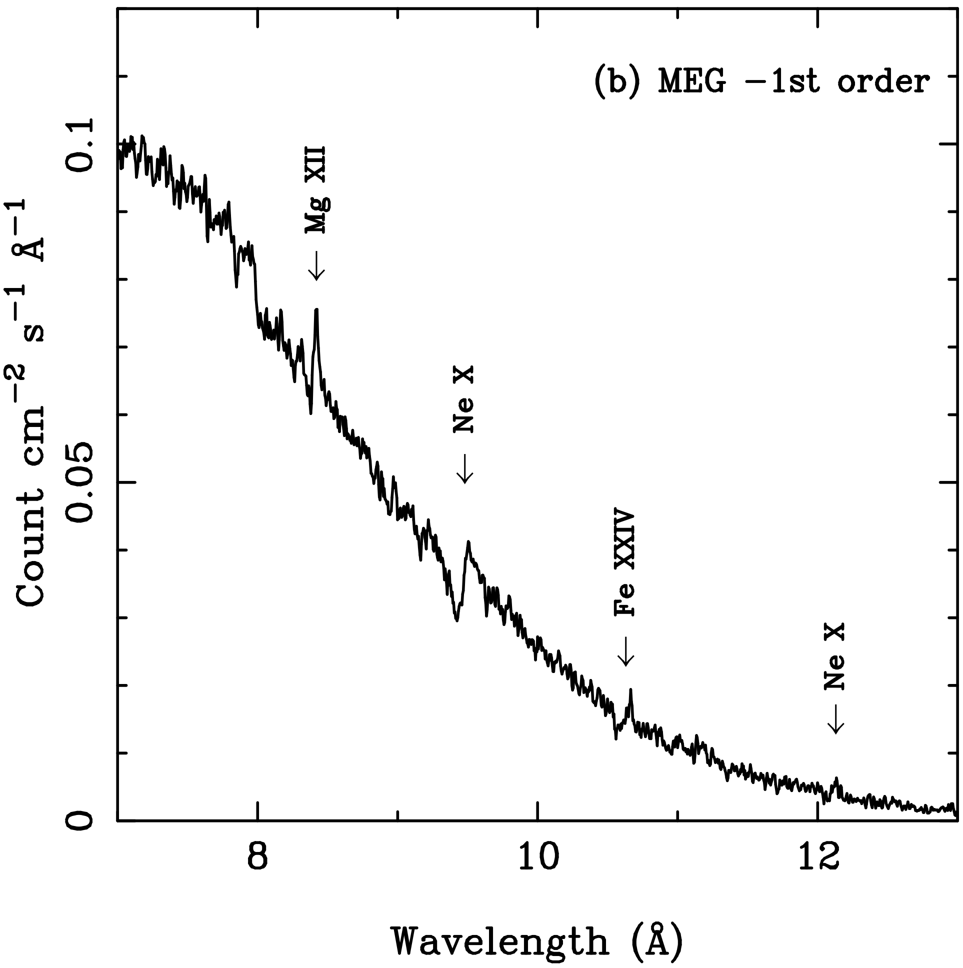

(b) MEG −1st order
Mg XII
Ne X
Fe XXIV
Ne X
Count cm^{-2} s^{-1} Å^{-1}
Wavelength (Å)
0
0.05
0.1
8
10
12

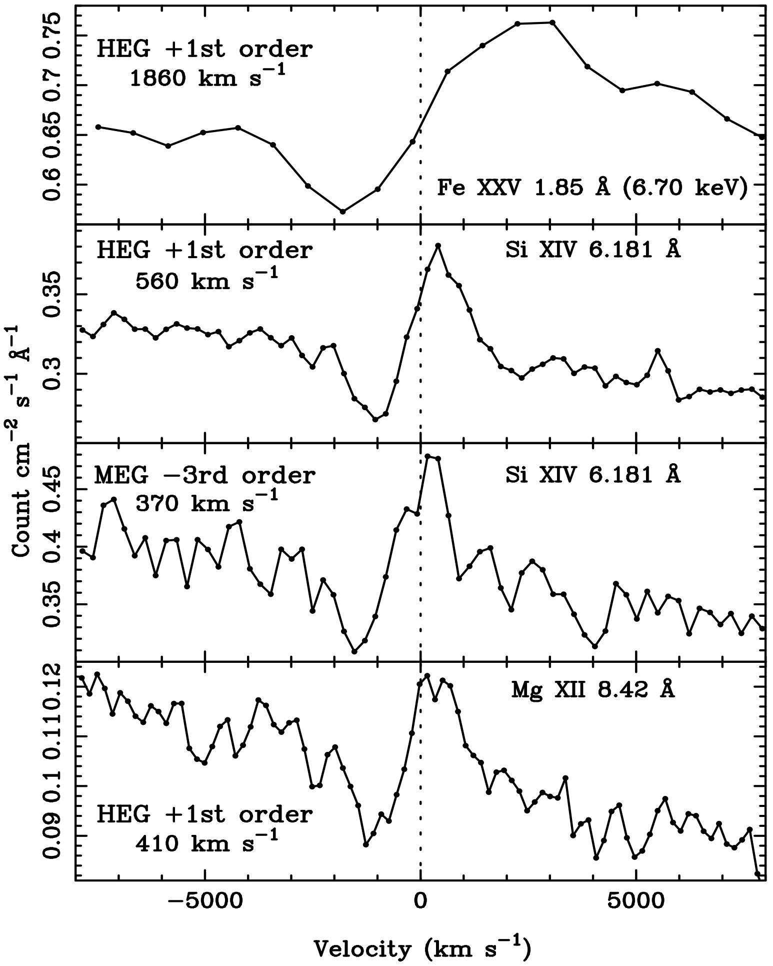

Fig. 3.— Velocity spectra showing the details of a few of the strongest X-ray P Cygni profiles seen from Cir X-1. We show the independent measurements of the Si XIV line from both the HEG +1st order and MEG −3rd order spectra. Typical bins in this figure have 200–1200 counts, and these spectra have not been smoothed. We list the relevant velocity resolution in each panel. The lines are clearly broader than the instrumental resolution with velocities of ± 2000 km s^{-1}, although the Fe XXV line is broadened by the instrument. We have taken zero velocity to correspond to the laboratory rest wavelength, since the radial velocity of Cir X-1 is not well established (Johnston et al. 1999 and H.M. Johnston 2000, private communication).